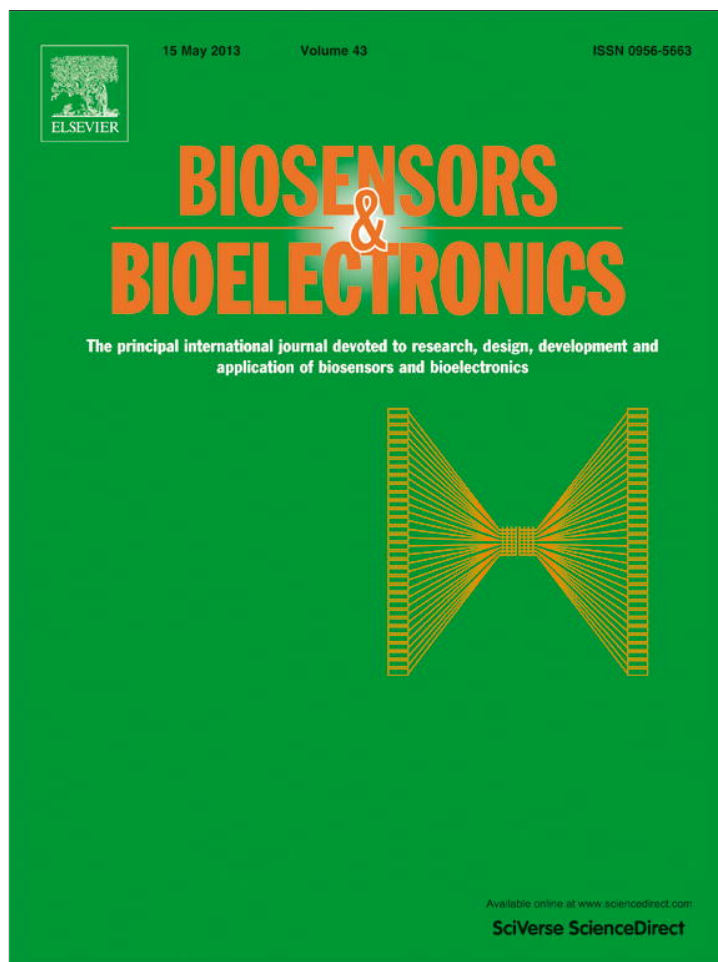


Provided for non-commercial research and education use.
Not for reproduction, distribution or commercial use.



This article appeared in a journal published by Elsevier. The attached copy is furnished to the author for internal non-commercial research and education use, including for instruction at the authors institution and sharing with colleagues.

Other uses, including reproduction and distribution, or selling or licensing copies, or posting to personal, institutional or third party websites are prohibited.

In most cases authors are permitted to post their version of the article (e.g. in Word or Tex form) to their personal website or institutional repository. Authors requiring further information regarding Elsevier's archiving and manuscript policies are encouraged to visit:

<http://www.elsevier.com/copyright>

Contents lists available at [SciVerse ScienceDirect](http://SciVerse.Sciencedirect.com)

Biosensors and Bioelectronics

journal homepage: www.elsevier.com/locate/bios

Real-time, in situ DNA hybridization detection with attomolar sensitivity without amplification using $(\text{pb}(\text{Mg}_{1/3}\text{Nb}_{2/3})\text{O}_3)_{0.65}-(\text{PbTiO}_3)_{0.35}$ piezoelectric plate sensors

Wei Wu^a, Ceyhun E Kirmli^b, Wei-Heng Shih^a, Wan Y. Shih^{b,*}^a Department of Materials Science and Engineering, Drexel University, Philadelphia, PA 19104, USA^b School of Biomedical Engineering, Science and Health Systems, Drexel University, Philadelphia, PA 19104, USA

ARTICLE INFO

Article history:

Received 21 November 2012

Accepted 19 December 2012

Available online 31 December 2012

Keywords:

Piezoelectric

Hybridization

Detection

DNA

Real-time

Sensitivity

ABSTRACT

In this paper we have investigated real-time, in situ DNA hybridization detection using piezoelectric plate sensors (PEPSs) consisting of a highly piezoelectric lead magnesium niobate-lead titanate (PMN-PT) layer 8 μm in thickness thinly coated with Cr/Au electrodes and electrically insulated with 3-mercaptopropyltrimethoxysilane (MPS) encapsulation. With probe complementary DNA (cDNA) immobilized on the PEPS surface and by monitoring the first longitudinal extension mode (LEM) resonance frequency shift of the PEPS we detected hybridization of the target DNA (tDNA) to the probe cDNA on the PEPS surface in real time at concentration 1.6×10^{-18} M with a signal to noise ratio of 8 without isolation and amplification at room temperature in 30 min in phosphate buffered saline (PBS) solution. The detection was validated in situ by two different methods: (1) the detection of fluorescently labeled microspheres coated with reporter cDNA complementary to the tDNA but different from the probe cDNA; (2) fluorescent visualization.

© 2012 Elsevier B.V. All rights reserved.

1. Introduction

Since the discovery of the structure of the deoxyribonucleic acid (DNA), detailed genetic analysis of diseases has become possible. The advance in modern genetic detection and genetic analysis has allowed the linkage of diseases with genes on the molecular level. As a result, we now know that many diseases including cancer are genetic and/or epigenetic in origin and that the same cancer may have different genetic and epigenetic pathways and more than one DNA markers.

It is also known that these genetic biomarkers of diseased cells are circulating in blood streams (Butt and Swaminathan, 2008; Holdenrieder et al., 2008a, 2008b; Holdenrieder and Stieber, 2004; Schwarzenbach H Fau – Hoonet al.; Tsang and Lo, 2007). Detecting circulating or cell-free DNA markers from blood—also known as “liquid biopsy”—can be a powerful method for disease diagnostics and prognostics. The challenge of detecting circulating target DNA (tDNA) is the low concentration of the tDNA, which often requires an analytic sensitivity at least in the attomolar (10^{-18} M or 1000 copies/ml) range (Caruso et al., 1997). Polymerase chain reaction (PCR) is the current gold standard for genetic detection. However, it requires gene isolation

and amplification. Nor is it rapid or low-cost or readily available for the general public. For disease screening and personalized medicine, the ability to rapidly detect multiple genetic markers and examine the genetic profile of the disease at low cost is greatly needed. For infectious disease, many bacteria have developed multiple-antibiotics resistant strains due to decades of exposures to various antibiotics. The ability to interrogate the genetic makeup of bacteria simply and rapidly would allow more timely treatment of the infections.

Current genetic detection technologies under development rely on fluorescence (Hammond et al., 2007), quartz crystal microbalance (QCM) (Passarnano and Pighini, 2006) (Feng et al., 2007) electrochemical (Gasparac et al., 2004) binding to nano-metal particles (Park et al., 2002), surface plasmon resonance (SPR) (He et al., 2000), silicon-based microcantilever sensor as well as piezoelectric microcantilever sensor (Rijal and Mutharasan, 2007; Zheng et al., 2011). For DNA detection, QCM exhibited a concentration sensitivity of 0.1 nM (Passarnano and Pighini, 2006). Direct conductivity measurement of metal nanoparticles exhibited a concentration sensitivity of 500 fM (Gasparac et al., 2004). The SPR exhibits concentration sensitivity of ~ 10 pM (He et al., 2000). The electrochemical methods also exhibit concentration sensitivity on the order of 1 pM (Feng et al., 2007) Nanowires (Zheng et al., 2005) and nanotubes (Wang et al., 2003b); (Chang et al., 2007; Kurkina et al., 2011) exhibit concentration sensitivity ranging from 100 fM to 0.2 fM. Microcantilevers coupled with nano-metal

* Corresponding author. Tel.: +1 215 8952 325.

E-mail address: shihwy@drexel.edu (W.Y. Shih).

particles exhibited 0.01 nM concentration sensitivity (Su et al., 2003). Although many of these methods such as QCM, SPR, silicon-based microcantilever sensor as well as lead zirconate titanate (PZT) piezoelectric microcantilever sensor (Rijal and Mutharasan, 2007) (Zheng et al., 2011) are label-free, the sensitivity is still many orders of magnitude away from the attomolar requirement. Similarly, the 10^{-16} M sensitivity achieved by magnetic beads isolation coupled with electrochemical enhancement was not sufficient (Wang et al., 2003a). Although nano-scale mechanical imaging by atomic force microscopy (AFM) can differentiate unhybridized single-stranded DNAs (ssDNAs) from hybridized double-stranded DNAs (dsDNAs) at attomolar level it requires sophisticated instrument such as AFM (Husale et al., 2009). Although several recent studies showed attomolar sensitivity detection, they were not label-free. For example, carbon nanotubes exhibited attomolar sensitivity using streptavidin horseradish peroxidase labeling for signal amplification (Gao et al., 2011). Electrochemical biosensor involving magnetic beads exhibited attomolar sensitivity using target DNA biotinylation (Loaiza et al., 2008) or electrocatalytic amplification (Soleymani et al., 2009). GaN nanowire based extended-gate field-effect-transistor exhibited attomolar real-time sensitivity (Chen et al., 2011) requiring the dilution of the buffer more than 100 times, indicating that the sensitivity before dilution was only 0.1 fM.

In this paper, we examine the detection sensitivity of lead magnesium niobate–lead titanate ($\text{Pb}(\text{Mg}_{1/3}\text{Nb}_{2/3})\text{O}_3)_{0.65}-(\text{PbTiO}_3)_{0.35}$ (PMN-PT) piezoelectric plate sensor (PEPS) in real-time, label-free, in situ DNA hybridization detection in full buffer solutions without isolation and amplification. PMN-PT PEPS is a new type of piezoelectric sensor consisting of a PMN-PT free-standing film 8 μm in thickness (Shih et al., 2006) thinly coated with gold electrodes on the two major surfaces and encapsulated with a thin electrical insulation as schematically shown in Fig. 1(a). Receptor specific to a biomarker is immobilized on the surface of the electrical insulation layer. Binding of the target biomarker to the receptor on the PEPS surface shifts the PEPS length-extension-mode (LEM) (Fig. 1(b)) or width-extension-mode (WEM) (Fig. 1(c)) resonance peak frequency, f . Detection of a target protein or DNA marker is achieved by directly immersing a PEPS in the biological fluid and monitoring the LEM or WEM resonance frequency shift, Δf in real time. For this study, we use HBV 1762/1764 double mutation (HBV DM) as the target DNA. HBV is a double mutation of a hepatitis B viral DNA variant comprised of adenine –1762 to thymine transversion and guanine –1764 to adenine transition which has been previously shown to be a risk factor for the development of Hepatocellular Carcinoma (HCC)

(Munoz et al., 2011; Yuan et al., 2009). A high percentage (> 60%) of HCC patients had HBVDM in their sera (Arbuthnot and Kew, 2001; Kuang et al., 2004).

In our earlier studies, we have shown that the relative detection resonance frequency shift, $\Delta f/f$, of a PMN-PT piezoelectric microcantilever sensor (PEMS), the predecessor of the PEPS, consisting of a PMN-PT layer bonded with a nonpiezoelectric layer such as copper or tin was enhanced (Zhu et al., 2008a) by the polarization switching capability of the PMN-PT layer (Hsieh et al., 2009) and was inversely proportional to the thickness of the PEMS (Shih et al., 2008). Polarization switching was the main underlying mechanism of the high piezoelectric performance of a morphotropic-phase-boundary (MPB) piezoelectrics such as PMN-PT (Park and Shrout, 1997; Shang and Tan, 2001) and PZT (Randall et al., 1998; Tsurumi et al., 2004). This indicates that a thin PMN-PT PEPS with a high piezoelectric coefficient could have greatly enhanced detection sensitivity. What makes the PMN-PT PEPS different from the PZT PEMS used in the earlier DNA detection studies is that the PMN-PT layer in the PMN-PT PEPS is both thin (8 μm) and highly piezoelectric. In comparison, the PEMS in a recent paper (Rijal and Mutharasan, 2007) used commercial PZT which was much thicker (127 μm). On the other hand, although the PZT layer from a recent study (Zheng et al., 2011) was thin its piezoelectric coefficient was only a fraction of that of the bulk PZT due to the fact that the film was made on a silicon substrate. Because of the combination of the high piezoelectric coefficient of the PMN-PT layer and its thinness a PEPS can achieve high detection sensitivity.

In the following, we will use the electromechanical coupling coefficient, k_{31} , (which characterizes the efficiency of converting the electrical energy associated with an electric field in the “3” direction to mechanical energy with deformations in the “1” direction and vice versa) to characterize the piezoelectric property of a PEPS. We will show that PMN-PT PEPS such as the one shown in Fig. 1(d) made with well sintered PMN-PT film with a high $-k_{31}$ of 0.32 (with a grain size of about 3–4 μm as shown in Fig. 1(e)) coated with 16mer probe complementary DNA (cDNA) can directly detect the 200-nucleotide (nt) target tDNA, HBV 1762/1764 DNA label-free, in situ in full buffer at a concentration of 1.6×10^{-18} M (100 copies/100 μl) in < 30 min without isolation or amplification. Such high concentration sensitivity was a result of > 1000 times enhancement in the detection relative resonance frequency shift $-\Delta f/f$ in the PMN-PT PEPS; Shih et al., 2008). The binding-induced elastic modulus change was a result of polarization switching in the PMN-PT layer upon binding of the target analyte; Shih et al., 2008). As resonance frequency was

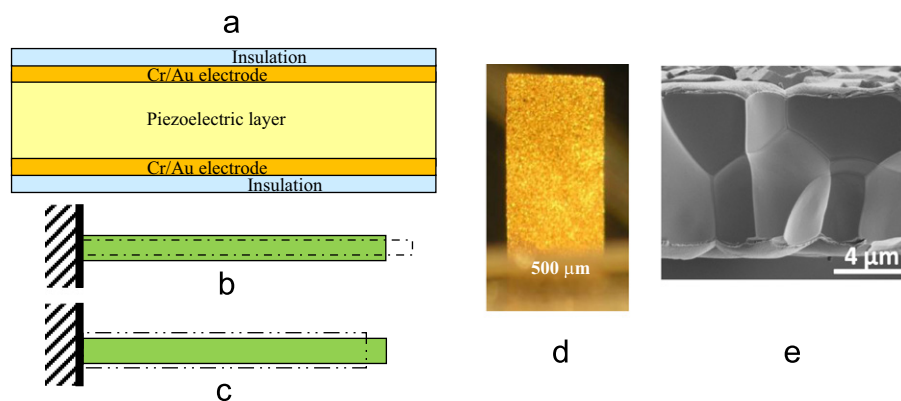


Fig. 1. A schematic of (a) a piezoelectric plate sensor (PEPS), (b) the first length extension mode (LEM), (c) width extension mode (WEM) vibration of a PEPS where the shaded bars illustrated the initial position of the PEPS and the dash-dotted shapes illustrate the extended positions, (d) a top-view optical micrograph and (e) a cross-section view scanning electron microscopy (SEM) micrograph of the PMN-PT PEPS used in this study. The gold color in (d) and the thin layers lining the top and the bottom of the PMN-PT are 110 nm Cr/Au electrodes and the microstructure in (e) indicates the grain size in this PMN-PT is about 4 μm . (For interpretation of the references to color in this figure legend, the reader is referred to the web version of this article.)

directly proportional to the square root of the elastic modulus (see Eq. (3)), the binding induced elastic modulus change gave rise to resonance frequency change orders of magnitude larger not accountable by mass change alone; Shih et al., 2008). This makes the current thin, soft PMN-PT PEPS different from all other nonpiezoelectric sensors and weakly piezoelectric sensors (such as quartz) that do not exhibit such binding-induced elastic modulus change.

2. Experimental procedure

2.1. PEPS fabrication

A 100 nm thick gold electrode was deposited on both sides of the PMN-PT film with a 10 nm chromium bonding layer by thermal evaporator (Thermionics VE 90). The gold-coated PMN-PT films were then cut into $600\text{--}1000 \times 2300 \mu\text{m}$ rectangular strips using a wire saw (Princeton Scientific Precision, Princeton, NJ). Gold wires 10 μm in diameter were then attached to the top and the bottom electrodes using conductive glue (8331, MG Chemicals). The rear end of the strip was then glued to a glass slide to form the final plate geometry. The strips were then poled at 15 kV/cm and 80 °C for 30 min on a hotplate. Five PEPS were used in this study. Each PEPS was 8 μm thick, about 1600 μm long, and 700 μm wide with one of the long ends fixed on a glass substrate (Fig. 1(d)). The dielectric constant of the PEPS was measured using an Agilent 4294 A electrical impedance analyzer (Agilent) to be about 1800 with a loss factor of 2–3.5% at 1 kHz. Fig. 1(e) shows the example SEM cross-section micrograph of the PEPSs used in this experiment that had a grain size of about 3–4 μm and a high $-k_{31}$ of about 0.32.

2.2. Electrical insulation

For electrical insulation, a PEPS was first cleaned in a 1-in-40 diluted piranha solution (two parts of 98% sulfuric acid (Fisher) with one part of 30% hydrogen peroxide (Fisher)) for 10 min followed by de-ionized (DI) water and ethanol (Fisher) rinsing. It was then soaked in a 0.1 mM 3-mercaptopropyltrimethoxysilane (MPS) (Sigma) in ethanol for 30 min followed by soaking in a 1% MPS in ethanol at pH 5.5 for 48 h. The MPS coating solution was replaced with a fresh one every 12 h. Each time the PEPS was first rinsed with DI water and ethanol before it was placed in the fresh MPS solution. The thickness of the MPS insulation layer was estimated to be $168 \pm 24 \text{ nm}$ according to the earlier thickness measurement using quartz crystal microbalance (QCM) (Capobianco et al., 2007). Finally, the PEPS is rinsed in DI water and ethanol and stored in a closed container before further surface modification and detection.

After insulation, the resonance spectra of the PEPS were measured using an Agilent 4294A electrical impedance analyzer (Agilent). The phase-angle-versus-frequency resonance spectra of the PEPS in air (black) and in phosphate buffer saline (PBS) solution (red) are shown in Fig. 2(a).

2.3. Probe cDNA immobilization

The targeted sequence of the HBV 1762/1764 double mutation tDNA is shown in Table 1 provided in the supplemental information with the two mutated nucleotides underlined. The probe cDNA immobilized on the PEPS surface was 5'-ACAAAGATCAT-TAACC-3' and biotin-activated at the 5'. The conjugation was carried out at room temperature. First, the PEPS was soaked in a 2 μM aqueous Maleimide-PEG₁₁-Biotin (Pierce) solution for 30 min followed by rinsing with DI water and phosphate buffer

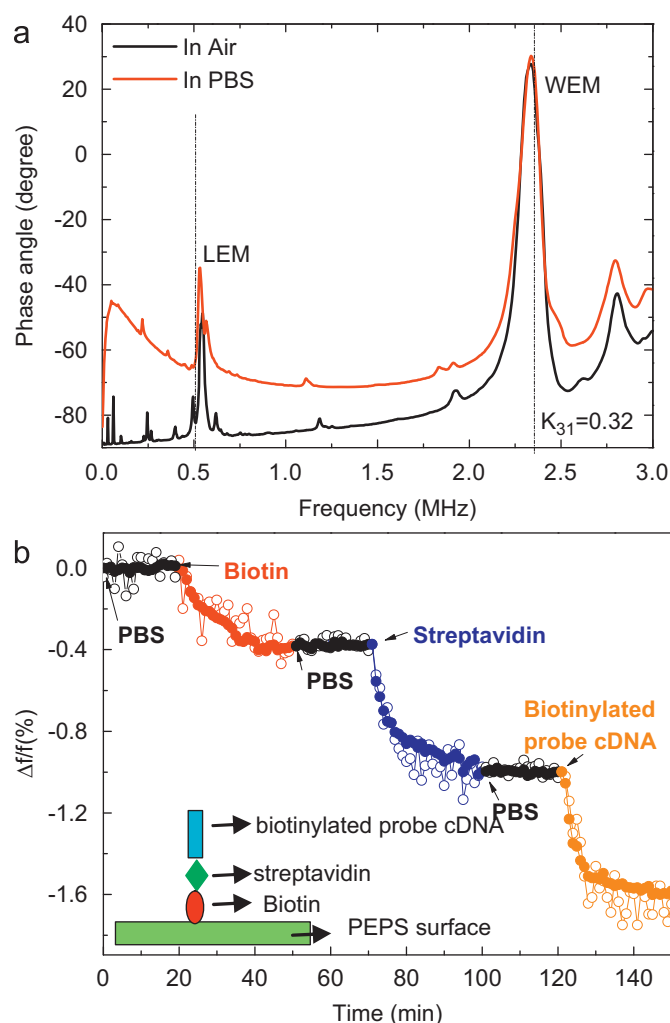


Fig. 2. (a) In-air (black) and in-PBS (red) phase angle-versus-frequency resonance spectra, and (b) relative resonance frequency shift, $\Delta f/f$, of the PMN-PT PEPS during the various steps of probe cDNA immobilization. The insert in (b) shows a schematic of the molecules involved in the immobilization. (For interpretation of the references to color in this figure legend, the reader is referred to the web version of this article.)

saline (PBS) solution (Mediatech). The biotin-functionalized PEPS was then soaked in a 10 mg/ml streptavidin (RayBiotech) solution in PBS for 30 min followed by DI water and PBS rinsing. Finally, the streptavidin-coated PEPS was soaked in a 2 μM biotinylated probe cDNA solution for 30 min. The relative resonance frequency shift, $\Delta f/f$, of the first LEM peak at various steps of the immobilization process is shown in Fig. 2(b). Also shown in the insert in Fig. 2(b) is a schematic of the various steps involved in the immobilization process. The details of the reaction steps of the immobilization can be found in the supplemental information. As can be seen, biotin, streptavidin, and the probe cDNA respectively generated a $\Delta f/f$ of 0.4%, 0.6%, and 0.6% after 30 min of binding. Once the PEPS was successfully coated with probe cDNA (as judged by the $\Delta f/f$ generated by the three steps described above), the PEPS was then subject to tDNA detection in a flow.

2.4. PEPS reuse

After each detection, a PEPS was regenerated as follows. First, it was cleaned with a 1:40 diluted piranha solution, and rinsed with DI water and ethanol. It was then re-soaked in a 1% MPS solution in ethanol at pH 5.5 overnight. Following the MPS

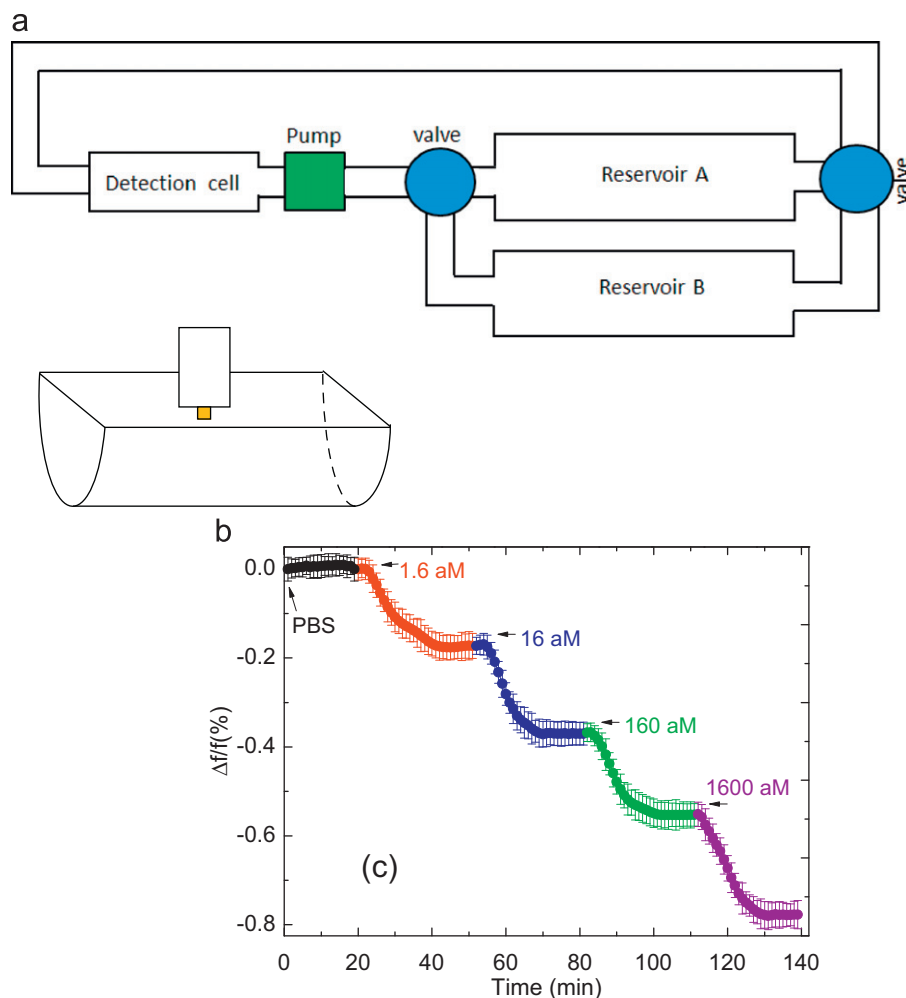


Fig. 3. A schematic of (a) the flow system, (b) the detection cell where the PEPS was placed vertically in the center of the flow with the major faces of the PEPS parallel to the flow, and (c) relative resonance frequency shift, $\Delta f/f$ versus time of tDNA detection with consecutively increasing concentrations at a flow rate of 1 ml/min. (For interpretation of the references to color in this figure legend, the reader is referred to the web version of this article.)

coating step, the probe cDNA was then immobilized as described above.

2.5. Flow setup

All the tDNA detections were carried out in a flow. A schematic of the flow system consisting of a polycarbonate detection chamber 18.5 mm long 3.5 mm wide and 5.5 mm deep (volume = 356 μ l), two reservoirs, and a peristaltic pump (Cole-Parmer 77120-62) interconnected with 2 mm wide tubing is shown in Fig. 3(a). The PEPS was vertically placed in the center of flow in the detection chamber with its major faces parallel to the flow (see Fig. 3(b)). In each detection event, only one reservoir is connected to the detection chamber. The total volume of the liquid was about 53–55 ml including the liquid in the reservoir, the detection chamber and the connecting tubing. Once the detection involving the first reservoir was over, the second reservoir was switched on and the first reservoir switched off to start the detection with the second solution. If there is a third solution following the second, the first reservoir was then replaced with a reservoir containing the third solution so that it could be switched on when the detection with the second solution was over. By doing so, the PEPS could sample different solutions while the resonance frequency of the PEPS could be continually monitored in situ to record the resonance frequency shift in real time. It is worth mentioning that the present

detection cell is an open one, switching from one fluid to another too quickly could generate a spike (either upward or downward) in the resonance frequency shift (not shown). However, we found that as long as the valves were turned slowly enough (> 20 s), switching from one solution to another did not generate a spike in the resonance frequency shift. We have also examined the effect of the flow rate to the detection. We found that if the flow rate was lower than 1 ml/min the detection response was reduced due to the lower number of target molecules flowing past the sensor per unit time. However, when the flow rate was higher than 1 ml/min, the flow started to generate noises in the resonance spectrum of the PEPS, increasing the noise level in the detection resonance frequency shift. Therefore, in the following, all detections were carried out with a flow rate of 1 ml/min corresponding to an average flow velocity of 1.4 mm/s at the PEPS surface.

3. Results and Discussions

3.1. In-air and in-PBS resonance spectra

The fundamental LEM and WEM resonance frequency of the PEPS was related to its length, L , and width, w , as

$$f_w = c/4L, \quad (1)$$

and

$$f_w = c/2w, \quad (2)$$

where L and w are respectively the length of the PEPS as measured from the free end to the glue line (see Fig. 1(d)) and the width of the PEPS, and

$$c = \sqrt{Y_{11}/\rho}, \quad (3)$$

is the sound velocity of the PMN-PT, and Y_{11} and ρ are the lateral Young's modulus and density of PMN-PT, respectively. Note that the numerical factor "4" in the denominator of Eq. (1) reflects that in the longitudinal direction one end of PEPS is always a fixed (nodal) point. The PEPS whose spectra are shown in Fig. 2(a) is 1605 μm long and 690 μm wide. The calculated LEM and WEM peak frequencies using Eqs. (1) and (2) with $Y_{11}=81$ GPa and $\rho=7800$ kg/m³ are shown as the vertical dashed lines in Fig. 2(a). As can be seen, the resonance peak of at 505 kHz corresponded to the first LEM peak and the strong resonance peak at 2.2. MHz corresponded to the first WEM resonance peak.

It is also worth noting that the frequency and height of the LEM peak and that of the WEM peak were not much affected by the immersion of the PEPS in the PBS. This is in strong contrast to the case of the flexural-mode in which both peak height and peak frequency were lowered by the liquid due to the damping effect as well as the inertia of the liquid moving in phase with the device (Shih et al., 2001). That the LEM and WEM peak frequencies were essentially unaffected by the liquid may be attributed to the negligible LEM (WEM) vibration amplitude, ΔL (Δw), which was only around 2 nm under the 100 mV applied voltage across the thickness of the PEPS during a typical resonance spectrum scan as estimated by $\Delta L = Ld_{31}(V/t)$ ($\Delta w = wd_{31}(V/t)$) where $-d_{31}=200-250$ pm/V was the piezoelectric coefficient of the PMN-PT layer relating the strain in the lateral direction to the electric applied in the thickness direction (Zhu et al., 2008a, 2008b). Because of the small LEM vibration amplitudes, the amount of liquid moving in phase with the PEPS was negligible. In comparison, the vibration amplitude at the tip of a flexural mode would be larger than 125 nm due to the L/t amplification factor where t is the thickness of the PEPS (Zhu et al., 2008a). That both the heights and the positions of the LEM and WEM peaks were mostly retained in liquid indicates that the LEM or WEM peaks were more suitable than the lower-frequency flexural modes whose peak heights were much lowered in PBS. The baseline of the spectrum in PBS was higher than that of the in-air spectrum presumably due to the conduction of the ions in the solution as a result of imperfect electrical insulation (A more detailed study of the shift of the baseline in liquid in relation to the electrical insulation coating will be examined in a future study).

3.2. Resonance frequency shifts during immobilization steps

To minimize the effect of instrumental noise in determining the resonance frequency, instead of using the highest phase angle value of a peak, we fitted a resonance peak to a simple parabola. The maximum of the fitted parabola was then recorded as the resonance frequency. As an example, the relative resonance frequency shift versus time measured in situ during the various immobilization steps is shown in Fig. 2(b) where the open symbols indicate the resonance frequency shift obtained from the raw resonance spectra and full symbols the resonance frequency shift obtained from the fitted parabola spectra. As can be seen, during the first 20 min in PBS, the fitted resonance frequency did not exhibit a significant shift; when exposed to a 2 μM of Maleimide-PEG-Biotin at $t=20-50$ min, the resonance frequency decreased and saturated at a $\Delta f/f$ (Δf) of about -0.4% (-2.0 kHz). At $t=50-70$ min, when the PEPS was rinsed with PBS

again, there was again no significant frequency shift. At $t=70-100$ min, when exposed to a 10 mg/ml streptavidin solution, the $\Delta f/f$ (Δf) resonance further decreased by about 0.6% (3.0 kHz) to a cumulative shift of about -1% (-5.0 kHz). The PEPS was then rinsed with PBS for 20 min and then exposed to a 2 μM biotinylated probe cDNA solution. Again, there was no significant resonance shift during the PBS rinsing at $t=100-120$ min while during the cDNA immobilization step at $t=120-150$ min, there was a $\Delta f/f$ (Δf) of about -0.6% (-3.0 kHz) which brought the cumulative $\Delta f/f$ (Δf) to about -1.6% (-8 kHz) at $t=150$ min. Note in all three PBS steps, no significant resonance frequency shifts were detected and the resonance frequency decreased and the resonance frequency shifts saturated in all three immobilization steps (i.e., biotin, streptavidin, and cDNA immobilization steps) as expected due to the high concentrations of these reagents chosen for immobilization. Note in all these three steps, the raw data went up and down around the fitted data, indicating that the parabola fitting algorithm was reasonable for removing some of the noise present in the system. In the following, all resonance frequency shifts were obtained from the fitted resonance peak unless otherwise mentioned.

To illustrate the enhancement effect due to the highly piezoelectric nature of the PEPS on the detection resonance frequency shift, we examine the cumulative $-\Delta f/f=1.6\%$ for the Maleimide-PEG₁₁-Biotin, streptavidin, and biotinylated probe DNA binding steps in Fig. 2(b) as an example. Maleimide-PEG₁₁-Biotin was 5.9 nm in length. The size of streptavidin was about 5 nm and the length of the 16-mer probe DNA was about 5.4 nm given the average nucleotide length is 0.34 nm. Altogether, the three layers were about 16.3 nm. If the effect of the Maleimide-PEG₁₁-Biotin, streptavidin, and biotinylated probe DNA binding on the PEPS surface was purely due to mass, the negative relative frequency shift, $(-\Delta f/f)_{\text{mass}}$ would be equal to the relative length change, $\Delta L/L$, which would be 1.02×10^{-5} given that ΔL equaled approximately the total thickness of the three layers ($L=1.605$ mm). As can be seen, the experimental $(-\Delta f/f)_{\text{exp}}$ was 1.6%, about 1000 times larger than the $(-\Delta f/f)_{\text{mass}}=1.02 \times 10^{-5}$ deduced from the mass effect. **This illustrates that the PEPS used in the above study with a $-k_{31}=0.32$ exhibited a $-\Delta f/f$ about 1000 times more than could be accounted for by the mass effect as a result of the high piezoelectric performance of the PMN-PT PEPS.** Note that among the three molecules involved in the probe cDNA immobilization, streptavidin was close to neutral and hence most appropriate to be used for the estimation of the number of molecules bound on the surface using QCM. A separate QCM measurement which gave about 60 Hz shift for the streptavidin binding step in a 5 MHz QCM (not shown) with which we estimated that there was about 1 streptavidin per 16 nm² on the PEPS surface. There were still three remaining binding sites left in the bound streptavidin, which likely would bind 1-2 amine activated probe cDNA. Therefore, we estimate that the density of the probe cDNA on the PEPS surface is likely 1 per 8–16 nm².

3.3. tDNA detection in consecutively increasing tDNA concentrations

Following the probe cDNA immobilization, we subject the PEPS to target tDNA detection. All tDNA detections were conducted in a flow at 28 °C in an incubator with humidity control. The first set of detections was done with the tDNA concentration increasing every 30 min starting with the flow of PBS for 20 min. The result of such detection at 1.6, 16, 160, 1600 aM (10^{-18} M) is shown in Fig. 3(c). The data shown in Fig. 3(c) were the average of 4 independent detections. As can be seen, the PEPS exhibited a $\Delta f/f$ of about -0.2% at 1.6 aM of tDNA but no significant resonance frequency shift in PBS. Furthermore, the PEPSs showed a $\Delta f/f$ of about -0.2% for each subsequent concentration increase. Note that with the standard

deviation in PBS—which was 0.025%—as the noise, the signal (S) to noise (N) ratio, S/N , was about 8 at 1.6 aM.

3.4. tDNA detection—dose response

The second set of detection was dose-response study where each detection experiment was only carried out at one tDNA concentration for 30 min. The tDNA concentration, c , ranged from 0, 1.6, 16, 160, 1600, to 16,000 aM. The relative resonance frequency shift $\Delta f/f$ versus time at various tDNA concentrations is shown in Fig. 4(a). Four different negative controls were carried out to make sure the observed relative resonance frequency shift, $\Delta f/f$, was indeed due to the hybridization of the tDNA with the probe cDNA but not nonspecific bindings. (1) Control 1 had the PEPS coated with probe cDNA in a buffer solution with no tDNA. (2) Control 2 had the PEPS coated with probe cDNA in a solution of 1.6 fM non-complementary DNA. (3) Control 3 had the PEPS without probe cDNA in a solution of 1.6 fM tDNA. (4) Control 4 had the PEPS with non-complementary cDNA in a solution with 1.6 fM tDNA. As can be seen, all four negative controls exhibited negligible $\Delta f/f$ in 30 min. On the other hand, there was a clear nonzero $\Delta f/f$ for every nonzero tDNA concentration at $t=30$ min and that $-\Delta f/f$ increased with an increasing tDNA concentration, indicating that the observed $\Delta f/f$ for nonzero tDNA concentrations was indeed due to the hybridization of the tDNA to the probe cDNA. Note that the data points shown in Fig. 4(a) were the average of 3–4 independent detection results. In Fig. 4(b), we plot the $-\Delta f/f$ at $t=30$ min versus tDNA concentration. Also shown in Fig. 4(b) is the S/N ratio at $t=30$ min where S was the $-\Delta f/f$ at $t=30$ min and N the standard deviation of $-\Delta f/f$ at zero tDNA concentration, c . As can be seen, both $-\Delta f/f$ and S/N increased with an increasing concentration logarithmically and that the $-\Delta f/f$ of 0.2% and S/N of about 8 at 1.6 aM were consistent with those obtained in Fig. 3(c), with $-\Delta f/f$ of 0.19%.

3.5. Visual validation using fluorescently labeled tDNA

To validate that the detected $\Delta f/f$ was indeed due to the hybridization of the target tDNA with the cDNA on the PEPS surface, we flowed 50-nt fluorescently-labeled tDNA (vendor) solution through the detection chamber instead of the 200-nt tDNA for 30 min. The PEPS was then rinsed with DI water three times to remove unbound tDNA. The fluorescent images of the bound fluorescent tDNA on the PEPS after the hybridization experiments at various fluorescent-tDNA concentrations as obtained in a fluorescent microscope (Olympus BX51) are shown in Fig. 4(c). As can be seen, the orange fluorescence of the dye could be clearly seen at tDNA concentrations $\geq 1.6 \times 10^{-14}$ M and the fluorescence increased with an increasing tDNA concentration, indicating that the probe cDNA was indeed immobilized on the PEPS surface and capable of capturing target tDNA from the solution.

3.6. In situ and visual validation with fluorescent microspheres

To validate in situ and by visualization after the detection, we follow the detection of the 200-nt tDNA with detection of fluorescently-labeled (Bright Blue, excitation: 360 nm, emission: 407 nm) microspheres (Polysciences) 6 μm in diameter conjugated with two 30-nt amine-activated reporter cDNAs with a 12-carbon spacer (Sigma) that were complementary to the tDNA but different from the probe cDNA on the PEPS surface. One reporter cDNA was complimentary to the sequence downstream and the other complementary to the upstream of the targeted sequence in the target tDNA as schematically shown in Fig. 5(a). The sequences of the reporter cDNAs are also shown in Table 1 in the Supplementary information. First, 0.1 ml of 2.1×10^8 particles/ml stock suspension of microspheres was diluted 10 times in PBS. Afterward, the suspension went through the following washing steps three times:

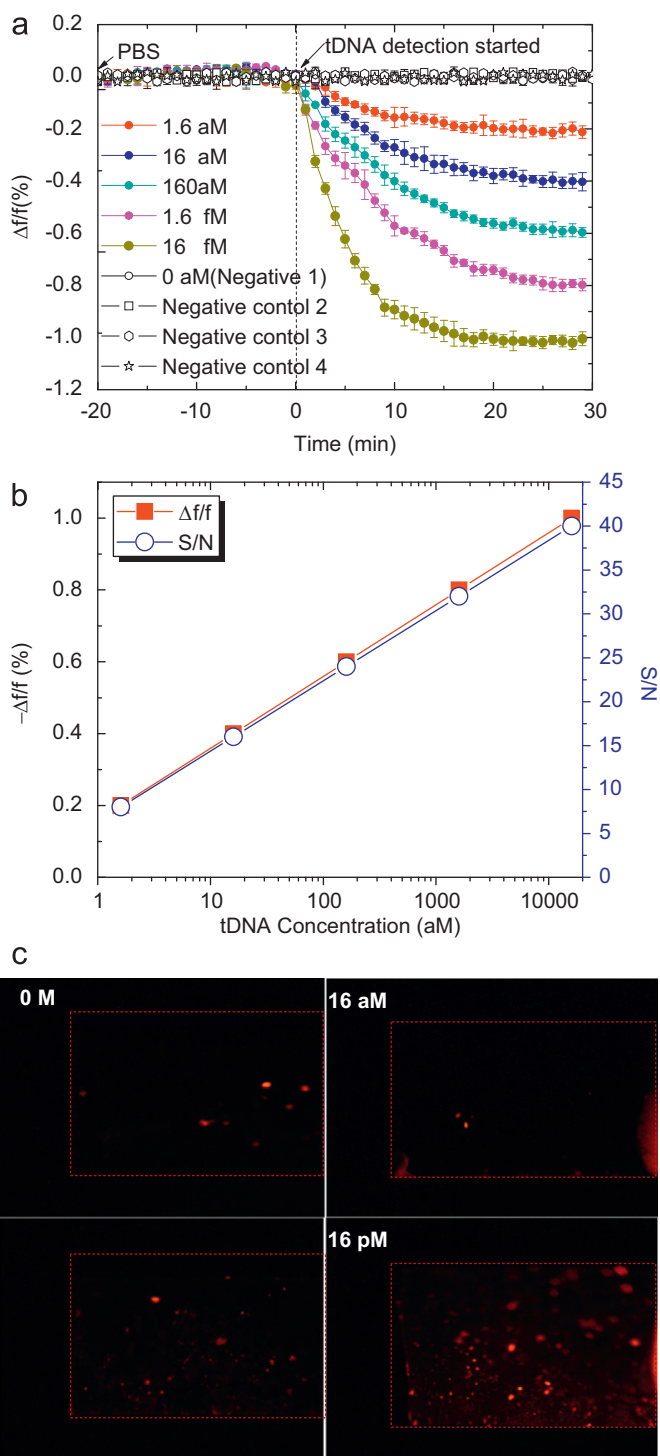


Fig. 4. (a) Relative resonance frequency shift versus time of the four controls together with the dose response of tDNA: open diamond for control 1 (probe cDNA, no tDNA); open squares for control 2 (probe cDNA, non-complementary DNA); open hexagons for control 3 (no cDNA, 1.6 fM tDNA); open stars for control 4: (non-complementary DNA, 1.6 fM tDNA), red circles, blue circles, green circles, pink circles, and olive circles for a probe cDNA coated PEPS in a 1.6 aM, 16 aM, 160 aM, 1.6 fM, and 16 fM, respectively, and (b) $-\Delta f/f$ at $t=30$ min (full squares) and signal/noise, S/N , ratio (open circles) versus tDNA concentration where the signal, S , was the $-\Delta f/f$ at $t=30$ min and the noise, N , was the standard deviation of $-\Delta f/f$ at zero tDNA concentration—Note all data points were the average of 3–4 independent runs, and (c) orange fluorescent images of the 50-nt fluorescently-labeled tDNA captured on the PEPS surface at various concentrations for 30 min—note the orange dashed lines were only to guide the eye for the boarder of the PEPS. The orange fluorescence exhibited at 16 fM and 16 pM and that the fluorescent signal increased with the tDNA concentration supported the resonance frequency shifts shown in (a) and (b) were due to the tDNA captured on the PEPS surface. (For interpretation of the references to color in this figure legend, the reader is referred to the web version of this article.)

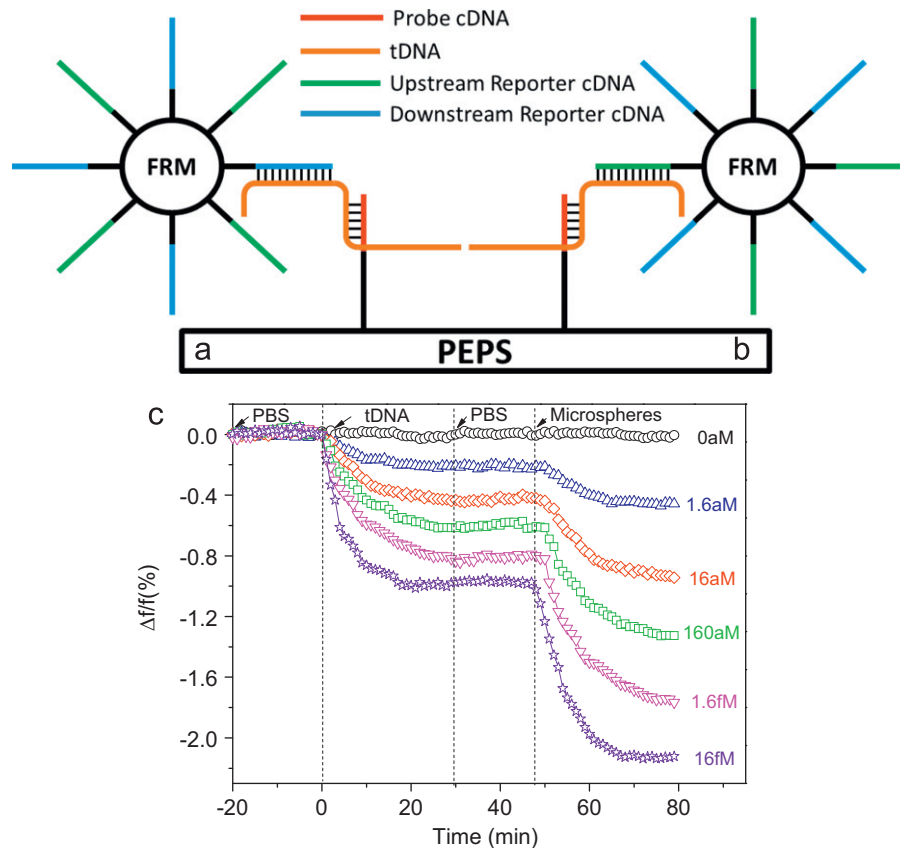


Fig. 5. A schematic of a microsphere conjugated to both upstream and downstream reporter cDNA to bind to a tDNA captured by a probe DNA on the PEPS surface via (a) a downstream reporter cDNA and (b) a upstream reporter DNA for both in situ validation and later visualization, (c) $\Delta f/f$ versus time of tDNA detection at various tDNA concentration at $t=0$ to 30 min followed with in situ validation by microsphere detection at $t=50$ –80 min.

vortexing for 15 s, centrifuging at 3700 rpm (Centra, CL2, IEC, MA), discarding the supernatant, re-suspending the sediment in 10 ml PBS. For conjugation, the suspension was mixed with 330 nM amine-activated upstream and downstream cDNAs mixed at a 1:1 ratio, 5 mg/ml 1-ethyl-3-(3-dimethylaminopropyl) carbodiimide (EDC) (Sigma, MA) and 5 mg/ml sulfonated *N*-Hydroxysuccinimide (sulfo-NHS) (Pierce, IL) and incubated at room temperature for 1 h. The details of the reaction schemes can be found in the [Supplementary information](#). The suspension was then washed by centrifugation 3 times as described above. After the final washing, a 10 ml of stock conjugated microspheres suspension of 2.1×10^6 particles/ml was obtained. For detection, 1 ml of the stock suspension of conjugated microspheres was further diluted by 10 times to a volume of 10 ml and a concentration 2.1×10^5 particles/ml. In the following, all the microspheres detection results were obtained at 2.1×10^5 particles/ml. Fig. 5(a) and (b) respectively show the schematics of a reporter microsphere conjugated to both upstream and downstream reporter cDNA to bind to a tDNA captured on a probe cDNA on the PEPS surface via a downstream reporter cDNA and an upstream reporter for both in situ validation and visualization.

In this study, 5 different PEPS were used to complete all the detection experiments. One PEPS was used to carry out the immobilization experiment shown in Fig. 2(b). The dose response results shown in Fig. 4(a) and (b) were carried out by two different PEPS. Another pair of PEPS was used to carry out the DNA hybridization detection and the subsequent FRMs validation detection shown in Fig. 5(b). The dose response curves shown in Fig. 4(a) were the average of 3–4 independent detections often carried out by two different PEPS. That the resultant dose response curves had reasonable standard deviations and the $\Delta f/f$

for the tDNA detection in Fig. 4(a) and Fig. 5(b) were quite similar indicated that the reproducibility of DNA hybridization detection among different PEPS.

In Fig. 5(c), we plot the $\Delta f/f$ versus time in tDNA detection at various tDNA concentrations followed by microspheres detection to validate PEPS tDNA detection in situ. A negative control was carried out to check that the microspheres do not have nonspecific binding when there is no tDNA on the PEPS surface (tDNA concentration is 0 aM in previous tDNA detection). As can be seen, flowing the microspheres after the initial tDNA detection produced a $\Delta f/f$ about the same magnitude for the tDNA detection. Since the reporters were complementary to the tDNA, the observation of the $\Delta f/f$ of the microspheres binding to the PEPS immediately after the tDNA detection served as in situ validation of the tDNA detection (much like the binding of the secondary antibody in an immunoassay). $\Delta f/f=0$ when tDNA is at 0 aM indicates that there is no nonspecific binding of microspheres.

In addition to the in situ validation, the fluorescently labeled microspheres are easy to observe in a microscope. We show the fluorescent images of the reporter microspheres captured on a PEPS surface following target detection at various tDNA concentrations in Fig. 6(a). As can be seen, the number of reporter microspheres increased with tDNA concentration in a dose response study further validating PEPS detection down to 1.6×10^{-18} M. To examine the number of microspheres observed on the PEPS and the $-\Delta f/f$ caused by the binding of the microspheres, we plot the $-\Delta f/f$ due only to the microspheres, i.e., the relative frequency shift between at $t=50$ and $t=80$ min in Fig. 6(b) (full squares) as well as the number of captured microspheres (open circles) obtained by counting the microspheres on

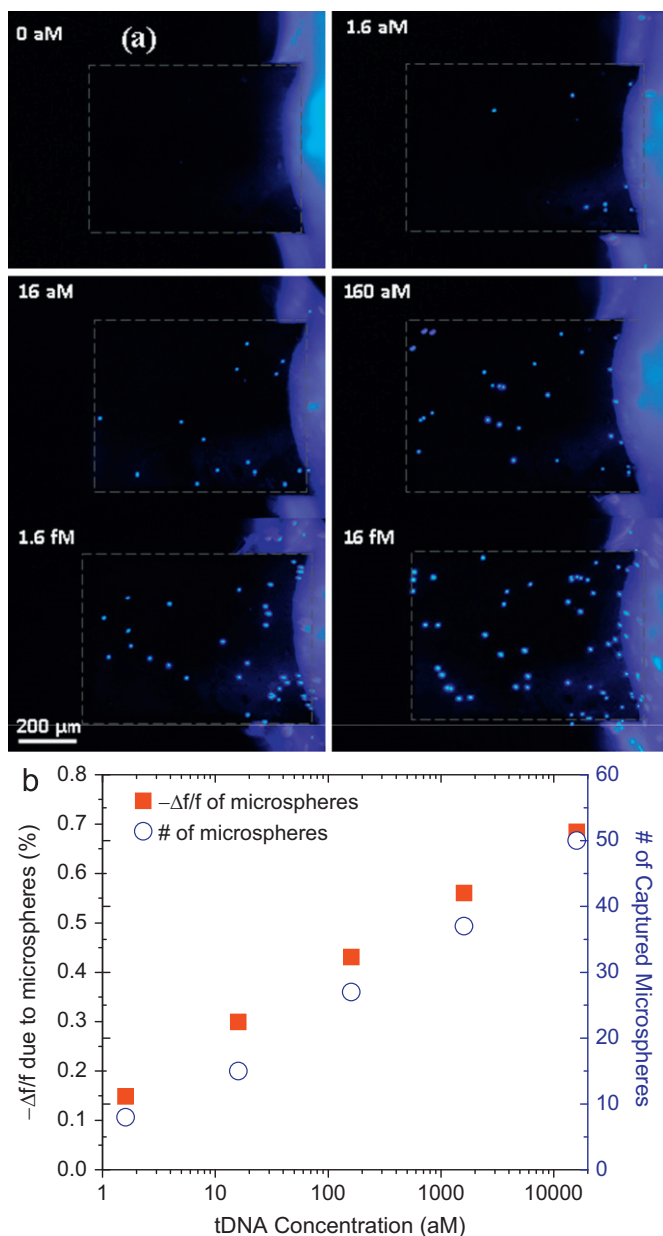


Fig. 6. (a) Blue fluorescent images of the captured microspheres on the PEPS surface after the microsphere detection following tDNA detection at various tDNA concentrations, and (b) $-\Delta f/f$ and the number of the captured microspheres versus tDNA concentration during the microsphere detection following the tDNA detection. (For interpretation of the references to color in this figure legend, the reader is referred to the web version of this article.)

one face of the PEPS in the microscope versus tDNA concentration. As can be seen, $-\Delta f/f$ was linear with the number of microspheres bound on the PEPS surface, supporting that PEPS resonance frequency shift was indeed reliable down to the aM tDNA concentration without isolation or amplification.

4. Conclusions

We have investigated real-time, in situ DNA hybridization detection using piezoelectric plate sensors (PEPSs) consisting of a highly piezoelectric lead magnesium niobate–lead titanate (PMN–PT) layer 8 μm in thickness thinly coated with Cr/Au electrodes and electrically insulated with 3-mercaptopropyltrimethoxysilane (MPS)

encapsulation. With probe complementary DNA (cDNA) immobilized on the PEPS surface and by monitoring the first longitudinal extension mode (LEM) resonance frequency shift of the PEPS we showed that we could detect hybridization of the target DNA (tDNA) to the probe cDNA on the PEPS surface at 1.6×10^{-18} M with a signal to noise ratio of 8 without isolation and amplification, which was validated in situ by the detection of fluorescently labeled microspheres coated with reporter cDNAs complementary to the tDNA but different from the probe cDNA following the detection of the tDNA and later by fluorescent visualization.

Acknowledgment

This work was supported in part by the Coulter–Drexel Translational Research Partnership Grant and the Nanotechnology Institute of Benjamin Franklin Partnership of Southeastern Pennsylvania.

Appendix A. Supporting information

Supplementary data associated with this article can be found in the online version at <http://dx.doi.org/10.1016/j.bios.2012.12.044>.

References

- Arbuthnot, P., Kew, M., 2001. *International Journal of Experimental Pathology* 82 (2), 77–100.
- Butt, A.N., Swaminathan, R., 2008. *Annals of the New York Academy of Sciences* 1137, 236–242.
- Capobianco, J.A., Shih, W.Y., Shih, W.H., 2007. *Review of Scientific Instruments* 78, 4.
- Caruso, F., Rodda, E., Furlong, D.N., Niikura, K., Okahata, Y., 1997. *Analytical Chemistry* 69 (11), 2043–2049.
- Chang, H.X., Yuan, Y., Shi, N.L., Guan, Y.F., 2007. *Analytical Chemistry* 79 (13), 5111–5115.
- Chen, C.-P., et al., 2011. *Analytical Chemistry* 83 (6), 1938–1943.
- Feng, K., Li, J.S., Jiang, J.H., Shen, G.L., Yu, R.Q., 2007. *Biosensors and Bioelectronics* 22 (8), 1651–1657.
- Gao, W., Dong, H., Lei, J., Ji, H., Ju, H., 2011. *Chemical Communications (Camb)* 47 (18), 5220–5222.
- Gasparac, R., Taft, B.J., Lapierre-Devlin, M.A., Lazareck, A.D., Xu, J.M., Kelley, S.O., 2004. *Journal of the American Chemical Society* 126 (39), 12270–12271.
- Hammond, D.M., Manetto, A., Gierlich, J., Azov, V.A., Gramlich, P.M.E., Burley, G.A., Maul, M., Carell, T., 2007. *Angewandte Chemie International Edition* 46 (22), 4184–4187.
- He, L., Musick, M.D., Nicewarner, S.R., Salinas, F.G., Benkovic, S.J., Natan, M.J., Keating, C.D., 2000. *Journal of the American Chemical Society* 122 (38), 9071–9077.
- Holdenrieder, S., Kolligs, F.T., Stieber, P., 2008a. *Clinical Chemistry* 54 (7), 1104–1106.
- Holdenrieder, S., Nagel, D., Schalthorn, A., Heinemann, V., Wilkowski, R., von Pawel, J., Raith, H., Feldmann, K., Kremer, A.E., Muller, S., Geiger, S., Hamann, G.F., Seidel, D., Stieber, P., 2008b. *Annals of the New York Academy of Sciences* 1137, 180–189.
- Holdenrieder, S., Stieber, P., 2004. *Annals of the New York Academy of Sciences* 1022, 211–216.
- Hsieh, C.Y., Chen, Y.F., Shih, W.Y., Zhu, Q., Shih, W.H., 2009. *Applied Physics Letters* 94, 13.
- Husale, S., Persson, H.H.J., Sahin, O., 2009. *Nature* 462 (7276), 1075–U1138.
- Kuang, S.Y., Jackson, P.E., Wang, J.B., Lu, P.X., Munoz, A., Qian, G.S., Kensler, T.W., Groopman, J.D., 2004. *Proceedings of the National Academy of Sciences of the United States of America* 101 (10), 3575–3580.
- Kurkina, T., Vlandas, A., Ahmad, A., Kern, K., Balasubramanian, K., 2011. *Angewandte Chemie International Edition England* 50 (16), 3710–3714.
- Loaiza, O.A., Campuzano, S., Pedrero, M., Pividori, M.L., Garcia, P., Pingarron, J.M., 2008. *Analytical Chemistry* 80 (21), 8239–8245.
- Munoz, A., Chen, J.G., Egner, P.A., Marshall, M.L., Johnson, J.L., Schneider, M.F., Lu, J.H., Zhu, Y.R., Wang, J.B., Chen, T.Y., Kensler, T.W., Groopman, J.D., 2011. *Carcinogenesis* 32 (6), 860–865.
- Park, S.E., Shrout, T.R., 1997. *Journal of Applied Physics* 82 (4), 1804–1811.
- Park, S.J., Taton, T.A., Mirkin, C.A., 2002. *Science* 295 (5559), 1503–1506.
- Passarmano, M., Pighini, M., 2006. *Sensors and Actuators B—Chemical* 118 (1–2), 177–181.
- Randall, C.A., Kim, N., Kucera, J.P., Cao, W.W., Shrout, T.R., 1998. *Journal of the American Ceramic Society* 81 (3), 677–688.
- Rijal, K., Mutharasan, R., 2007. *Analytical Chemistry* 79 (19), 7392–7400.
- Schwarzenbach, H., et al., 2011. *Nature Reviews Cancer* 11(6), 426–437.

- Shang, J.K., Tan, X., 2001. *Acta Materials* 49 (15), 2993–2999.
- Shih, W.Y., Li, X.P., Gu, H.M., Shih, W.H., Aksay, I.A., 2001. *Journal of Applied Physics* 89 (2), 1497–1505.
- Shih, W.Y., Luo, H.Y., Li, H.D., Martorano, C., Shih, W.H., 2006. *Applied Physics Letters* 89, 24.
- Shih, W.Y., Zhu, Q., Shih, W.H., 2008. *Journal of Applied Physics* 104, 7.
- Soleymani, L., Fang, Z., Kelley, S.O., Sargent, E.H., 2009. *Applied Physics Letters* 95 (14), 143701–143703.
- Su, M., Li, S.U., Dravid, V.P., 2003. *Applied Physics Letters* 82 (20), 3562–3564.
- Tsang, J.C., Lo, Y.M., 2007. *Pathology* 39 (2), 197–207.
- Tsurumi, T., Sasaki, T., Kakemoto, H., Harigai, T., Wada, S., 2004. *Japanese Journal of Applied Physics* 43 (11A), 7618–7622.
- Wang, J., Kawde, A.N., Musameh, M., 2003a. *Analyst* 128 (7), 912–916.
- Wang, J., Polsky, R., Merkoci, A., Turner, K.L., 2003b. *Langmuir* 19 (4), 989–991.
- Yuan, J.M., Ambinder, A., Fan, Y., Gao, Y.T., Yu, M.C., Groopman, J.D., 2009. *Cancer Epidemiology, Biomarkers & Prevention: A Publication of the American Association for Cancer Research, Cosponsored by the American Society of Preventive Oncology* 18 (2), 590–594.
- Zheng, G.F., Patolsky, F., Cui, Y., Wang, W.U., Lieber, C.M., 2005. Multiplexed electrical detection of cancer markers with nanowire sensor arrays. *Nature Biotechnology* 23 (10), 1294–1301.
- Zheng, S., Choi, J.H., Lee, S.M., Hwang, K.S., Kim, S.K., Kim, T.S., 2011. *Lab Chip* 11 (1), 63–69.
- Zhu, Q., Shih, W.Y., Shih, W.H., 2008a. *Applied Physics Letters* 92, 18.
- Zhu, Q., Shih, W.Y., Shih, W.H., 2008b. *Applied Physics Letters* 92, 3.